International Journal of Heat and Technology
Vol. 42, No. 5, October, 2024, pp. 1517-1524
Journal homepage: http://iieta.org/journals/ijht

Numerical Investigation of Flow and Thermal Fields in Heat Exchanger with Two Porous Vertical Baffles

Anas Alwatban

Department of Mechanical Engineering, College of Engineering, Qassim University, Qassim 51452, Saudi Arabia

Corresponding Author Email: a.alwatban@qu.edu.sa

https://doi.org/10.18280/ijht.420504

Received: 8 June 2024
Revised: 14 September 2024
Accepted: 29 September 2024
Available online: 31 October 2024

Keywords:
energy transfer, turbulent flow, modeling, porous vertical baffles, skin friction coefficient, thermal energy, performance assessment, heat exchanger

ABSTRACT

The turbulent airflow in a rectangular channel with two porous vertical baffles of 25%, 50%, and 75% porosity is investigated using the finite volume method and Fluent software. The k-ε turbulence model analyzes turbulence dynamics, adjusting boundary conditions for varying inlet velocities. Key parameters, including turbulent kinetic energy (TKE), dynamic pressure (DP), temperature variation (T), friction coefficient (Cf), Nusselt number (Nu), and thermal enhancement factor (TEF) are evaluated at Reynolds numbers of 28,000 and 56,000. Findings indicate that at a Reynolds number of 28,000, the 25% porous ratio maximizes energy transfer, while the friction coefficient peaks at the same ratio for a Reynolds number of 56,000. Notably, the TEF reaches 1.4 at a 75% porous ratio for a Reynolds number of 28,000. This research uniquely demonstrates the pronounced impact of porous baffles on heat transfer and friction under different Reynolds numbers, particularly highlighting the significance of baffle porosity in lower Reynolds number regimes.

1. INTRODUCTION

1.1 Background information

Numerous researchers have investigated thermal development using passive and active techniques. The passive approach entails integrating vortex generators within heat exchangers to generate streams of vortices across heat transfer sections. These vortex streams instigate alterations in the thermal boundary layer, serving as the principal mechanism for enhancing heat transfer. Moreover, the vortex streams promote fluid mixing, improving heat transfer efficiency.

In contrast, the active technique supplements the heating process with external power to elevate the heat transfer rate. Although the active method achieves heightened efficiency in heat transfer, it concurrently escalates operational costs.

The passive technique for the present investigation has been selected to improve thermal performance and increase the heat transfer rate in the heat exchanger channel.

1.2 Literature review

Bekele et al. [1] studied the effect of delta-shaped baffles on the surface of the air heater. The delta baffle is situated at 90° relative to the absorber surface. In their study, the Reynold number values are variable. Also, the height and longitudinal placement of the delta-shaped baffles are varied. The best case in their study showed a 3.6 times enhancement in the heat transfer when Re = 7200, P/e = 3⁄2) and e/H = 0.75.

Saim et al. [2] explored the effect of inclined baffles on the heat transfer characteristics of solar air heaters. The baffles are fixed at an angle of 5° relative to the absorber plate. The channel has fixed baffles at both the top and bottom. The flow rate varies from Re = 12,000 to 38,000. Their results indicate that high velocities can be reached inside the channel, enhancing the heat transfer rate.

Mokhtari et al. [3] numerically studied the effect of different baffle models. Three models were used with the proper boundary conditions. The baffles are placed on top of the absorber plate. The baffle's orientation was changed based on the angle of the baffle relative to the flow direction. Their results show a 40 to 50% heat transfer enhancement in the laminar regime and 15 to 20% in the turbulent regime.

Naik and Tiwari [4] examined how the placement of vortex generators near fin-tube heat exchangers impacts their performance. The vortex generators' angle of attack was changed from 15° to 60°. Also, the Reynold number was varied from 2000 to 4000. More than 37% was enhanced compared to the case with no vortex generators.

Promvonge and Skullong [5] experimentally studied the effect of punched winglet corrugation shapes. The winglets had two shapes: delta and elliptical. The circular punches in the winglet were varied in four sizes. The flow rate was varied as Reynold number from 4000 to 25000. The results were compared with solid delta and elliptical winglets. It was shown that the punched delta winglet had the best thermal performance enhancement factor of 2.17.

Menni et al. [6] numerically studied modern V-shaped fins fitted along a solar duct air heater. The study focused on varying the fin's angle of attack, length, separation length, and flow rate. The optimum case was shown with the 40° angle of attack with a thermal enhancement factor of 2.163 when the

flow rate is high.

Alshwairekh [7] conducted a computational fluid dynamics study on novel two-term sine-wave corrugations. The corrugations were used in a flat plate heat exchanger. The sinewave can be produced with different amplitudes and frequencies. The findings showed that utilizing double sine wave corrugations can result in a 20% improvement in the Nusselt number and a 15% reduction in the friction factor. Also, the results suggest that low amplitude and low frequent corrugations will yield a better thermal enhancement factor.

Medjahed et al. [8] numerically studied the effect of inserting two T-shaped vortex generators in a solar channel heat exchanger. One is at the upper wall, and the other is at the bottom wall. The upper and bottom walls are fixed at constant temperatures. The paper's results indicated that the best thermal rate was obtained with the highest Reynold number. However, the pressure drop that occurred was significant.

Zhang et al. [9] studied both numerical and experimental investigation of the effect of ribs and vortex generators on the heat transfer inside a rectangular channel. The study looked at four different types of ribs and vortex generators. The flow rate varies as Reynold's number varies from 20000 to 10000. Also, the winglet vortex generator was compared with the tetrahedral vortex generator. The paper's results show that the common flow-down winglet vortex generator showed the best thermal performance at all Reynold numbers.

Salhi et al. [10] numerically studied the effect of partially inclined baffles with variable height and changing the number of baffles on the heat transfer rate inside channels. The flow inside the channel is forced convection of air. The paper's results indicate that the heat transfer rate is enhanced by 59% with a Reynold number of 10,000 and that the height of the baffle is 3 cm. Also, increasing the baffle height with a high Reynold number will increase the heat transfer rate.

Batista et al. [11] numerically analyzed heat transfer behavior and fluid flow in an air-to-water fin and tube heat exchanger. They used winglet-type vortex generators on the air side to promote air mixing. Three different values of attack angles were used for the wiglet vortex generator. The delta-winglet downstream configuration with a 30° attack angle proved the best case regarding the heat transfer and pressure drop ratio.

Brahimi et al. [12] numerically studied the cooling of microprocessors by attaching air-cooled channels to them. The channel is filled with obstacles to promote mixing and enhance heat transfer. Square, trapezoidal, and triangular obstacles with different angles of attack were used. The results showed that the triangular case had the best cooling with a high Nusselt number and not an excessive pressure drop.

Brodniansk and Kotšmíd [13] performed numerical and experimental assessments on a wavy-shaped heated channel equipped with cylindrical vortex generators. They used the interferometry method to visualize the temperature field, and all the flow field properties were visualized using Ansys Fluent. The results showed that inserting cylindrical vortex generators is feasible in increasing the heat transfer while maintaining a relatively low-pressure drop.

Shlash and Koç [14] numerically studied the use of three different kinds of vortex generators in channels. Triangular, hale circle and quarter circle shapes have been used. The effect of the step height and the flow rate were changed to study their impact. The results show that the quarter circle shape had the best thermal-hydraulic performance at 4 mm step height.

Alwatban and Aljabr [15] numerically studied the inclusion of two obstacles along a channel with non-identical lengths. Sixteen cases of different sizes were studied with constant flow rates. The main results show that when the length of the second baffle is half the length of the first one, the thermal enhancement factor increases by 3%. The authors state that the obstacles should not be the same length.

The literature review above reveals that a considerable amount of experimental and numerical research has been conducted to investigate using longitudinal vortex turbulators to improve heat transfer. However, published studies are scarce exploring unique arrangement techniques for turbulent airflow within a rectangular cross-section channel equipped with two porous vertical baffle plates. This study aims to investigate the utilization of vortex generators for analyzing TKE, DP, T, *Cf*, *Nu* and TEF by incorporating two porous vertical baffle plates with varying porous ratios of 25%, 50%, and 75%. The research examines two distinct Reynolds numbers: 28,000 and 56,000.

2. MATHEMATICAL MODEL

The analysis assumes a two-dimensional, incompressible flow field, employing air as the working fluid with consistent physical properties. To effectively resolve this flow scenario through numerical methods, the essential governing equations encompass those governing continuity, momentum, and energy.

The incompressible flow under steady conditions is governed by the equation for mass conservation.

$$\frac{\partial(\rho u)}{\partial x}+\frac{\partial(\rho v)}{\partial y}=0 \tag{1}$$

The momentum equation is as follows in the x and y directions.

$$\frac{\partial(\rho u^2)}{\partial x}+\frac{\partial(\rho uv)}{\partial y} = -\frac{\partial P}{\partial x}+\frac{\partial}{\partial x}\left[(\mu_l+\mu_t)\left(\frac{\partial u}{\partial x}\right)\right] + \frac{\partial}{\partial y}\left[(\mu_l+\mu_t)\left(\frac{\partial u}{\partial y}\right)\right] \tag{2}$$

$$\frac{\partial(\rho uv)}{\partial x}+\frac{\partial(\rho v^2)}{\partial y} = -\frac{\partial P}{\partial y}+\frac{\partial}{\partial x}\left[(\mu_l+\mu_t)\left(\frac{\partial v}{\partial x}\right)\right] + \frac{\partial}{\partial y}\left[(\mu_l+\mu_t)\left(\frac{\partial v}{\partial y}\right)\right] \tag{3}$$

The energy equation is:

$$\frac{\partial(\rho uT)}{\partial x}+\frac{\partial(\rho vT)}{\partial y} = \frac{\partial}{\partial x}\left[\left(\mu_1+\frac{\mu_1}{\sigma_T}\right)\left(\frac{\partial T}{\partial x}\right)\right] + \frac{\partial}{\partial y}\left[\left(\mu_1+\frac{\mu_1}{\sigma_T}\right)\left(\frac{\partial T}{\partial y}\right)\right] \tag{4}$$

The equation for turbulent kinetic energy (k) is as follows:

$$\frac{\partial(\rho u k)}{\partial x}+\frac{\partial(\rho v k)}{\partial y} = \frac{\partial}{\partial x}\left[(\mu_l+\frac{\mu_t}{\sigma_k})\left(\frac{\partial k}{\partial x}\right)\right] + \frac{\partial}{\partial y}\left[(\mu_l+\frac{\mu_t}{\sigma_k})\left(\frac{\partial k}{\partial y}\right)\right]+G_k+\rho\varepsilon \quad (5)$$

The equation for turbulent kinetic energy (ε) is provided as follows:

$$\frac{\partial(\rho u \varepsilon)}{\partial x}+\frac{\partial(\rho v \varepsilon)}{\partial y} = \frac{\partial}{\partial x}\left[(\mu_l+\frac{\mu_t}{\sigma_\varepsilon})\left(\frac{\partial \varepsilon}{\partial x}\right)\right] + \frac{\partial}{\partial y}\left[(\mu_l+\frac{\mu_t}{\sigma_\varepsilon})\left(\frac{\partial \varepsilon}{\partial y}\right)\right]+G_{1\varepsilon}\frac{\varepsilon}{k} - G_{2\varepsilon}\rho\frac{\varepsilon^2}{k} \quad (6)$$

where,

$$\mu_t = \rho c_\mu k^2/\varepsilon \quad (7)$$

The definition of Reynolds-number that was used in the calculations based on the following:

$$Re = \frac{\rho u_{in} d_h}{\mu} \quad (8)$$

where, d_h is the hydraulic diameter of the channel, diameter and it is defined as:

$$d_h = \frac{2HW}{(H+W)} \quad (9)$$

The skin friction coefficient (C_f):

$$C_f = \frac{2\tau_w}{\rho u_m^2} \quad (10)$$

The friction coefficient (*f*):

$$f = \frac{(\Delta P/L)d_h}{\frac{1}{2}\rho \bar{U}^2} \quad (11)$$

The local Nusselt number:

$$Nu_x = h_x\frac{d_h}{k_f} \quad (12)$$

Nusselt number:

$$Nu = \frac{1}{L}\int Nu_x dx \quad (13)$$

The Petukhov correlation:

$$f_0 = (0.79\ln Re - 1.64)^{-2} \quad \text{for } 3\times10^3 \le \text{Re} \le 5\times10^6 \quad (14)$$

The Dittus-Boelter correlation:

$$Nu_0 = 0.023\, Re^{0.8} Pr^{0.4} \quad \text{for Re} \ge 10^4 \quad (15)$$

Thermal Enhancement Factor (TEF):

$$TEF = (Nu/Nu_o)/(f/f_0)^{1/3} \quad (16)$$

2.1 Geometry

Figure 1 illustrates the two-dimensional channel model, displaying the sizes of the two porous vertical perforated baffle plates located at the upper and lower walls of the channel. In this model, the channel measures 554 mm in length, 146 mm in height, and 193 mm in width. Two perforated vertical baffles with varying porosity ratios are employed. In all cases, the baffles maintain a height of 80 mm and a thickness of 10 mm. In Case (a-b), the dimensions are set as follows: s = 12 mm, e = 5 mm, with the total area of rectangular porosity comprising 25% of the baffle height. Case (c-d) features a 50% ratio, with s = 8 mm and e = 10 mm, while Case (e-f) adopts a 75% ratio, with s = 4 mm and e = 15 mm. The upper baffle is positioned 218 mm from the channel inlet, while the lower baffle is located 174 mm from the exit. Both baffles are parallel and separated by a horizontal distance of 142 mm across all three cases. Based on prior research, these baffle positions are chosen using solid vertical baffles or perforated plates [16-18]. Table 1 includes detailed information about the three cases for this research.

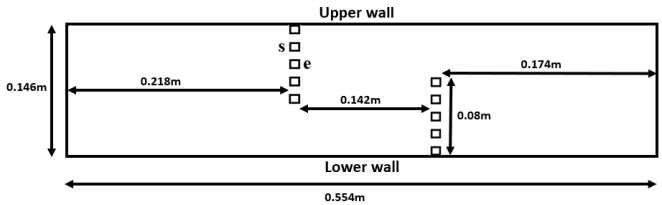

Figure 1. Schematics of the channel containing porous baffles and the dimensions

Table 1. Summary of three cases under study

Case	Re	s (mm)	e (mm)	s Total (mm)	e Total (mm)	Baffle Height (mm)
a	28,000	12	5	60	20	80
b	56,000	12	5			
c	28,000	8	10	40	40	80
d	56,000	8	10			
e	28,000	4	15	20	60	80
f	56,000	4	15			

2.2 Numerical model

Simulations are carried out using two different flow rates, resulting in Reynolds numbers of 28,000 and 56,000. The method examines the variations in velocity profile, skin friction coefficient, pressure drop, temperature, and turbulent kinetic energy within the analyzed channel. The inlet of the channel has fixed boundary conditions with constant values.

$$\begin{cases} u = U_{in} \\ v = 0 \\ T_{in} = 300\ K \\ k_{\text{in}} = 0.005\ U_{\text{in}}^2 \\ \varepsilon_{\text{in}} = 0.1\ k_{\text{in}}^2 \end{cases} \quad (17)$$

The outlet of the channel has fixed boundary conditions with constant values.

$$\begin{cases} \frac{\partial u}{\partial x} = 0 \\ \frac{\partial v}{\partial x} = 0 \\ \frac{\partial k}{\partial x} = 0 \\ \frac{\partial \varepsilon}{\partial x} = 0 \\ P = P_{\text{atm}} \end{cases} \quad (18)$$

The upper wall of the channel has fixed boundary conditions with constant values set.

$$\begin{cases} u = 0 \\ v = 0 \\ T = 375\ K \\ k = 0 \\ \varepsilon = 0 \end{cases} \quad (19)$$

The lower wall of the channel has fixed boundary conditions with constant values set.

$$\begin{cases} u = 0 \\ v = 0 \\ T = 0, Adiabatic \\ k = 0 \\ \varepsilon = 0 \end{cases} \quad (20)$$

The numerical model developed for fluid flow and heat transfer in the channel is grounded on several crucial assumptions. The model assumes that fluid properties remain constant throughout the domain and that velocity and temperature profiles are uniform at the channel's inlet. Moreover, it disregards body forces, viscous dissipation, and radiation heat transfer as negligible factors.

2.3 Mesh generation and validation

To mitigate the impact of grid distortion on the numerical solution, the quantity of mesh elements underwent adjustment from 10,000 to 60,000, incremented by 10,000. The influence of altering the density of elements on the mean axial velocity along the vertical axis at x=0.3 for case (f) is illustrated in Table 2 for a Reynolds number of 56,000.

Table 2. Variation of the average velocity case (f) at x=0.3 m for Re=56,000

Number of Elements	Average Velocity (m/s)
10,000	4.78
20,000	4.80
30,000	4.81
40,000	4.82
50,000	4.82
60,000	4.82

Following the mesh investigation detailed earlier, a uniform count of 40,000 elements was adopted for all cases. Figure 2 displays the mesh configuration encompassing the channel's entrance, two porous vertical baffles, and the channel's exit for case (f). This code has been previously employed in our earlier work by Alwatban and Othman [19], wherein validation against the experimental findings of Demartini et al. [20] demonstrated remarkable consistency.

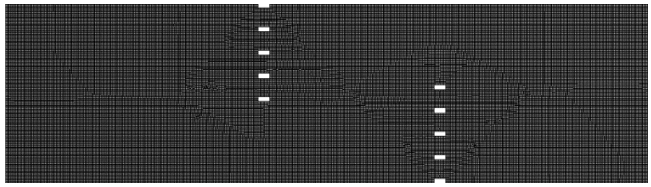

Figure 2. Sample of the mesh for the geometry with porous baffles

3. RESULTS AND DISCUSSION

This section explores the influence of porous ratios on various parameters such as TKE, DP, T, *Cf*, *Nu*, and TEF at two distinct Reynolds numbers (28,000 and 56,000).

Figure 3 illustrates the stream-wise velocity contours for all cases. For a porosity ratio of 25% in case (a-b), it was observed that the maximum velocity values were reached at the top section of the second baffle and the bottom section of the first baffle for both Reynolds numbers. A similar trend was observed with higher values at Re= 56,000. The maximum exit velocity was approximately 5.22 m/s for Re=28,000, while it increased to 11.35 m/s at a Reynolds number of 56,000 (more than 217%). Velocity values downstream of the rectangular holes for each baffle were also recorded to be higher, and these values increased with increasing inlet velocities. The presence of baffles altered the streamlines, with the first baffle directing the flow field into contact with the insulated lower wall, resulting in decreased pressure after the first baffle. It was observed that the length of the vortex was more affected by increasing the Reynolds number.

In case (c-d) with a porosity ratio of 50%, vortices were still observed below and above the first and second baffles, respectively. However, these vortices' intensity was significantly lower than those observed in cases (a-b). The maximum exit velocity reached 6.92 m/s for an inlet velocity of 4.9 (Re=56,000), while it was only 3.48 m/s for Re=28,000.

The effect was minimal in case (e-f) with a porosity ratio of 75%, and the maximum exit velocity reached 5.39 m/s for the higher Reynolds number. The presence of perforated baffles with different porosity ratios did not influence the dynamic behavior of the flow. However, the axial velocity increased with increasing inlet velocity values. Increasing the Reynolds number increased the axial flow velocity, as shown in Table 3.

Table 3. Summary of the axial velocity values for the three cases under study

Case	Re	u_{in} (m/s)	u_{exit_max} (m/s)	u_{exit_max}/u_{in}
a	28,000	2.45	5.22	2.13
b	56,000	4.90	11.35	2.32
c	28,000	2.45	3.48	1.42
d	56,000	4.90	6.92	1.41
e	28,000	2.45	2.83	1.15
f	56,000	4.90	5.39	1.10

Figure 4 depicts the vertical velocity contour plots along the channel at Re = 28,000 and 56,000 for the three cases under investigation. The vertical velocity diminished as the flow approached the first baffle. Additionally, it was observed that

in case (a-b), a sizable recirculation zone existed. Nevertheless, negative values were also noted downstream of the two baffles of varying sizes. In contrast, the velocity profile almost dropped to zero at the bottom of the channel. The upper perforated plate baffle induced a zone of negative velocities near the center of the channel. Increasing the Reynolds number extended the recirculation region. The region with the highest vertical velocities was situated upstream of the second baffle, affixed to the channel's bottom wall. It was observed that currents flowed positively toward the upper side of the channel. Moreover, the figure clearly illustrates that a large area was susceptible to rapid flow around the holes of each baffle. The vertical velocities at their maximum and in the negative direction showed values that were lower than the velocity contours in the axial direction. These observations were consistent across all three cases, with diminishing intensities as the porosity ratio increased and Reynolds number values decreased. For both Reynolds number values, it was revealed that the vertical velocity reached its maximum value at the second porous baffle near the upper wall of the channel. In contrast, its minimum value occurred at the first baffle near the bottom wall of the channel.

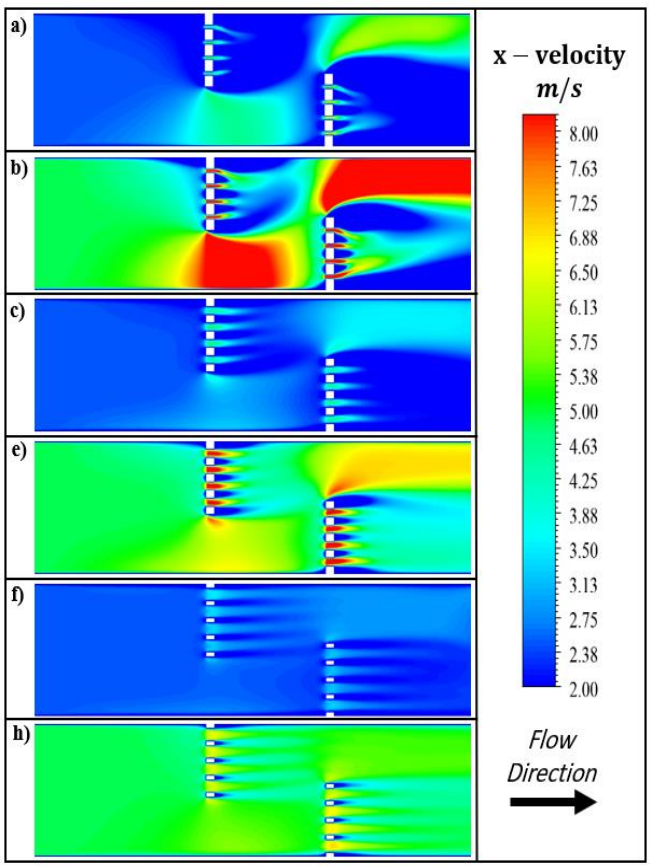

Figure 3. Contours of the stream-wise velocity for all cases

Significant dynamic pressure values were detected at various points within the channel walls. Figure 5 illustrates high dynamic pressure values near the top wall above the second porous baffle and the bottom wall below the first baffle. Additionally, substantial values were observed downstream of the rectangular holes. These dynamic pressure values increased as the Reynolds number increased, correlating closely with the axial velocity variation depicted in Figure 3. The dynamic pressure values rose across gaps due to a reduced flow area caused by obstacles.

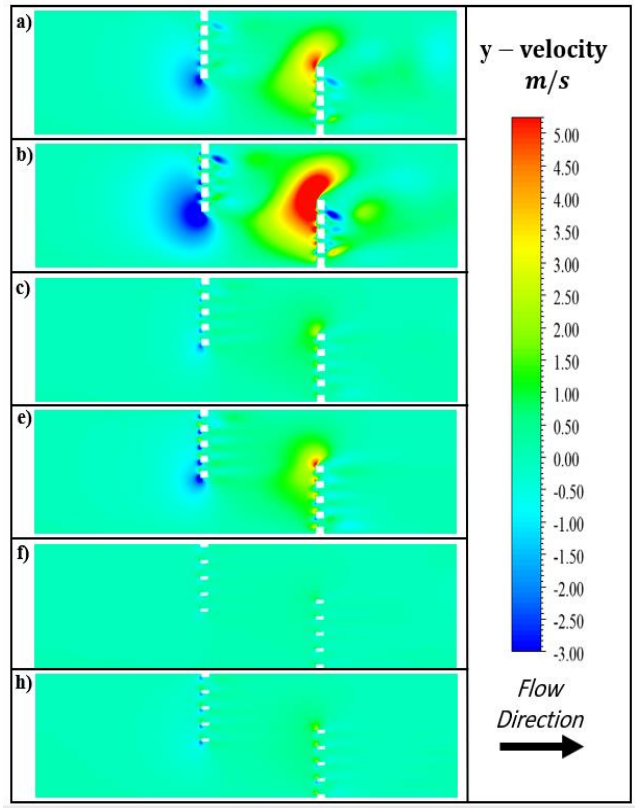

Figure 4. Contours of the vertical velocity for all cases

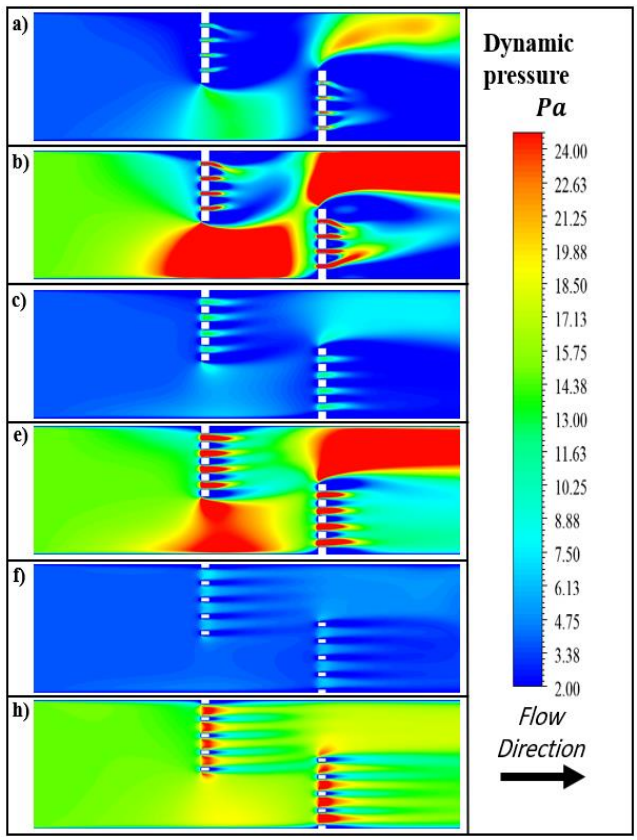

Figure 5. Contours of the dynamic pressure for all cases

The flow passes through gaps with elevated dynamic pressure, generating robust cells for recirculation due to a decline in dynamic pressure values on the rear surfaces of the barriers. Figure 5 illustrates that the recirculation cells grew taller, longer, and stronger as the Reynolds number increased.

Moreover, as the porosity ratio increased, the size of the dynamic pressure zones expanded, albeit with reduced intensity at the same Reynolds number values. Recirculation cells behind obstacles lead to low mean velocity (V) values (see Figure 3). Mean velocity values increased towards the upper and lower edges of the top and bottom baffles, respectively, owing to high dynamic pressure.

Figure 6 illustrates three distinct regions showcasing the variation in turbulent kinetic energy with both porosity ratio and Reynolds number values. The first zone, extending from the channel inlet to the first porous baffle, exhibits relatively minor turbulence levels with a nearly constant value; in the second region, located between the two porous vertical baffles, turbulent kinetic energy peaks at the bottom of the upper baffle and perforation exits. The distribution of turbulent kinetic energy is noteworthy near the channel's exit, representing the third region. As depicted in the figure, turbulent kinetic energy peaks at the center of the channel beneath the top baffle and spans nearly the entire channel upstream and downstream of the second porous baffle for the 25% porosity case (a-b) at a Reynolds number of 56,000. Conversely, turbulent kinetic energy values are lower in other parts of the channel. The figure indicates that higher Reynolds numbers increase kinetic energy for all three cases under investigation, particularly downstream of each baffle. The intensity and size of turbulent kinetic energy zones decrease with increased porosity ratio. These values are minimized for case (e-f) at a Reynolds number of 28,000. The observed trend in turbulent kinetic energy closely resembles the findings of Alqahtani et al. [21].

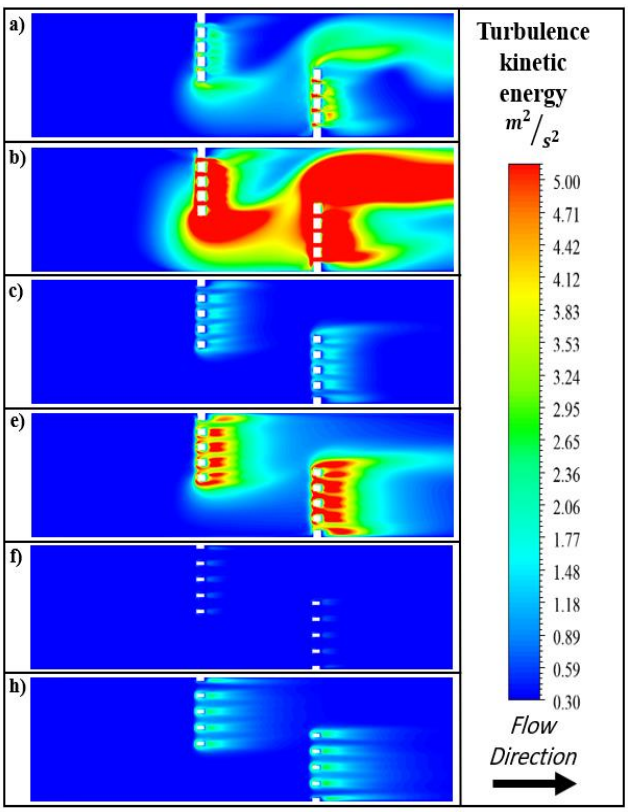

Figure 6. Contours of the turbulent kinetic energy for all cases

Figure 7 illustrates the variation in air temperature as it traverses through the channel. The channel's upper wall was kept at a temperature of 375 K, and it was assumed that the lower wall and all baffles were insulated. It was observed that the 25% porosity case (a-b) exhibited a broader zone of temperature gradient along the top wall and downstream of the upper baffle compared to cases (c-d) and (e-f). The addition of baffles greatly improves heat transfer by encouraging mixing and separating the boundary layer within the channel. This is the main way to enhance heat transfer in this system. An additional influential aspect is the ongoing formation of boundary layers and the dissipation of wakes. The changes in temperature closely match the patterns of axial velocity and dynamic pressure shown in Figures 3 and 5.

The ensuing discussion encompasses an analysis of heat transfer characteristics, including the normalized skin friction coefficient, absolute and normalized Nusselt numbers, and thermal enhancement factor. Table 4 presents the variations of these parameters at two Reynolds number values, 28,000 and 56,000, across the three cases under investigation: 25%, 50%, and 75% porosity ratios. The findings unveiled that as the porosity ratio increased, the normalized Nusselt number decreased. Moreover, the Nusselt number was found to rise as the Reynolds number values increased, which was consistent with established knowledge. As Reynolds number values escalate, the laminar sublayer thickness diminishes, consequently enhancing heat transfer owing to the presence of eddies and circulations induced by the baffles. Notably, the second baffle at the bottom wall yielded the highest normalized Nusselt number values, attributed to the heightened flow velocity.

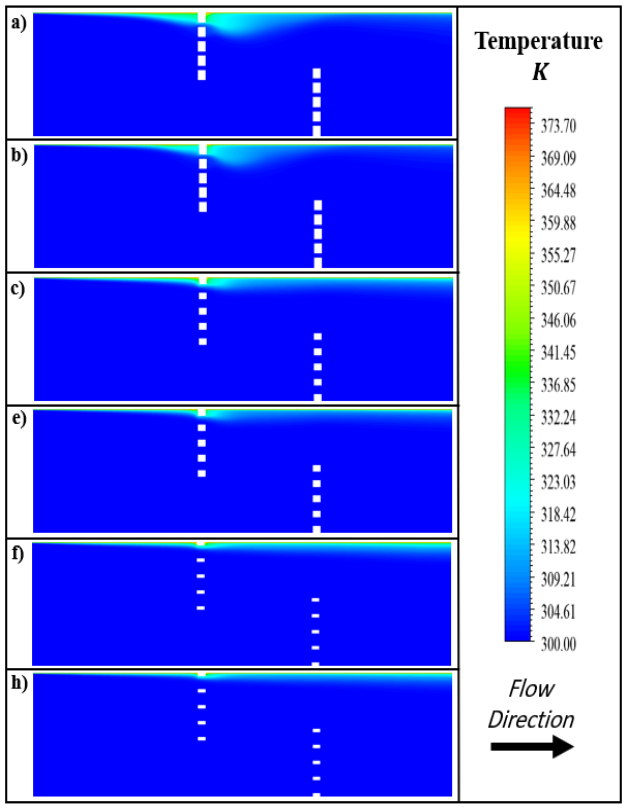

Figure 7. Contours of the temperature for all cases

The correlation between the friction coefficient, which amplifies pressure drop, and increased heat transfer is noteworthy. As depicted in Table 4, the normalized skin friction coefficient rose with higher Reynolds number values for identical porosity ratios. The highest recorded value, 35.77, was observed in case (a-b) at a Reynolds number of 56,000. Conversely, the normalized skin friction coefficient values

decreased with rising porosity ratios, with the lowest value, 2.39, noted in case (e) at a Reynolds number of 28,000. The intermediate zone between the baffles exhibited elevated values due to a recirculation zone.

Thermal enhancement factor (TEF) values surged with increasing porosity ratios but declined with escalating Reynolds numbers across all examined cases. Strengthened recirculation lengths were observed due to heightened thermal gradients at maximum velocity. The study highlights the preference for a porosity ratio of 75% (case e), as it yielded a 1.79 times increase in TEF compared to case (a) at a Reynolds number of 28,000.

Table 4. Summary of the $\frac{Nu}{Nu_s}$, $\frac{Cf}{Cf_s}$, and TEF variations for all cases

Case	Re	Nu	$Nu/_{Nu_s}$	$f/_{f_s}$	TEF
a	28,000	172.79	2.40	29.22	0.78
b	56,000	281.90	2.25	35.77	0.68
c	28,000	146.32	2.03	8.29	1.00
d	56,000	226.26	1.80	9.68	0.85
e	28,000	134.66	1.87	2.39	1.40
f	56,000	193.64	1.54	2.42	1.15

The rise in friction factor value resulting from the utilization of baffles can be attributed to the dynamic pressure dissipation of the fluid stemming from the increased surface area and flow obstruction. Generally, recirculation or reverse flow induces a significantly more significant friction factor increase than axial flow. Moreover, friction is generated through the expansion of the interaction area and dynamic pressure dissipation.

4. CONCLUSION

This study conducted a numerical examination of flow and thermal characteristics within a heat exchanger featuring two porous vertical baffle plates with three varying porosity ratios: 25%, 50%, and 75%. The dimensions of the baffles were set consistently at 80 mm in height and 10 mm in breadth across all cases. The analysis entailed solving differential equations for a two-dimensional channel using the finite volume method. The turbulence dynamics were elucidated by implementing the k-ε turbulence model through Fluent software. Adjustments were made to the boundary conditions of the inlet velocity field to evaluate the system comprehensively. The study aimed to investigate the influence of porosity ratios on TKE, DP, T, Cf, Nu, and TEF for two distinct Reynolds numbers (28,000 and 56,000). A mesh study was conducted to determine the consequence of the result. The number of elements was selected to be 40,000. The experimental data exhibited excellent comparability, confirming the model's validity.

The study reveals that at a Reynolds number of 28,000, the highest energy transfer is achieved with a 25% porous ratio, while at 56,000, the friction coefficient peaks with the same ratio. For a Reynolds number of 28,000, the thermal enhancement factor (TEF) is maximized at 1.4 with a 75% porous ratio (case e), indicating that the baffles have a more significant effect at lower Reynolds numbers. A notable correlation exists between increased friction coefficients and enhanced heat transfer. The normalized skin friction coefficient increases with Reynolds number, reaching 35.77 in case (a-b) at 56,000, but decreases with higher porosity ratios, with a minimum of 2.39 in case (e) at 28,000. TEF values rise with higher porosity but fall with higher Reynolds numbers. Overall, a 75% porosity ratio (case e) offers the most significant improvement in TEF, with a 1.79 increase compared to case (a) at a Reynolds number of 28,000.

Based on the findings of the current numerical simulation study, there are several recommendations for future research. These suggestions encompass, but are not limited to, the following:

1. The Reynolds numbers should be varied to cover a wider range of velocities at the inlet.
2. Instead of straight baffles, angled baffles could be used by altering their shape.
3. Additional baffles could be included within the same channel dimensions by adjusting the dimensions between the baffles.

REFERENCES

[1] Bekele, A., Mishra, M., Dutta, S. (2011). Effects of delta-shaped obstacles on the thermal performance of solar air heater. Advances in Mechanical Engineering, 3: 103502. https://doi.org/10.1155/2011/103502

[2] Saim, R., Bouchenafa, R., Benzenine, H., Oztop, H.F., Al-Salem, K., Abboudi, S. (2013). A computational work on turbulent flow and heat transfer in a channel fitted with inclined baffles. Heat and Mass Transfer, 49: 761-774. https://doi.org/10.1007/s00231-013-1121-3

[3] Mokhtari, M., Gerdroodbary, M.B., Yeganeh, R., Fallah, K. (2017). Numerical study of mixed convection heat transfer of various fin arrangements in a horizontal channel. Engineering Science and Technology, an International Journal, 20(3): 1106-1114. https://doi.org/10.1016/j.jestch.2016.12.007

[4] Naik, H., Tiwari, S. (2018). Effect of winglet location on performance of fin-tube heat exchangers with inline tube arrangement. International Journal of Heat and Mass Transfer, 125: 248-261. https://doi.org/10.1016/j.ijheatmasstransfer.2018.04.071

[5] Promvonge, P., Skullong, S. (2020). Enhanced heat transfer in rectangular duct with punched winglets. Chinese Journal of Chemical Engineering, 28(3): 660-671. https://doi.org/10.1016/j.cjche.2019.09.012

[6] Menni, Y., Ghazvini, M., Ameur, H., Ahmadi, M.H., Sharifpur, M., Sadeghzadeh, M. (2020). Numerical calculations of the thermal-aerodynamic characteristics in a solar duct with multiple V-baffles. Engineering Applications of Computational Fluid Mechanics, 14(1): 1173-1197. https://doi.org/10.1080/19942060.2020.1815586

[7] Alshwairekh, A.M. (2024). Thermal-hydraulic performance of additively manufactured plate heat exchangers with single and double sine wave corrugations: A CFD study. International Journal of Heat & Technology, 42(4): 1231-1239. https://doi.org/10.18280/ijht.420413

[8] Medjahed, D.M., Ameur, H., Rebhi, R., Inc, M., Ahmad, H., Menni, Y., Aldhabani, M. (2021). Details on the hydrothermal characteristics within a solar-channel heat-exchanger provided with staggered t-shaped baffles. Energies, 14(20): 6698. https://doi.org/10.3390/en14206698

[9] Zhang, G., Liu, J., Sundén, B., Xie, G. (2021). Combined experimental and numerical studies on flow characteristic and heat transfer in ribbed channels with vortex generators of various types and arrangements. International Journal of Thermal Sciences, 167: 107036. https://doi.org/10.1016/j.ijthermalsci.2021.107036
[10] Salhi, J.E., Mousavi Ajarostaghi, S.S., Zarrouk, T., Saffari Pour, M., Salhi, N., Salhi, M. (2022). Turbulence and thermo-flow behavior of air in a rectangular channel with partially inclined baffles. Energy Science & Engineering, 10(9): 3540-3558. https://doi.org/10.1002/ese3.1239
[11] Batista, J., Trp, A., Lenic, K. (2022). Heat transfer enhancement of crossflow air-to-water fin-and-tube heat exchanger by using delta-winglet type vortex generators. Energies, 15(6): 2070. https://doi.org/10.3390/en15062070
[12] Brahimi, A., Rebhi, R., Alliche, M. (2023). Numerical study of the effects of roughness coupled with Inclination on a turbulent flow around an obstacle. Processes, 11(7): 1979. https://doi.org/10.3390/pr11071979
[13] Brodnianská, Z., Kotšmíd, S. (2023). Heat transfer enhancement in the novel wavy shaped heat exchanger channel with cylindrical vortex generators. Applied Thermal Engineering, 220: 119720. https://doi.org/10.1016/j.applthermaleng.2022.119720
[14] Shlash, B.A.A., Koç, I. (2022). Turbulent fluid flow and heat transfer enhancement using novel Vortex Generator. Journal of Advanced Research in Fluid Mechanics and Thermal Sciences, 96(1): 36-52. https://doi.org/10.37934/arfmts.96.1.3652
[15] Alwatban, A., Aljabr, A. (2024). Thermo-flow behavior of air-channel heat exchanger with nonidentical baffle lengths: computational analysis. Journal of Thermal Analysis and Calorimetry, 149(8): 3593-3603. https://doi.org/10.1007/s10973-024-12906-1
[16] Shehab, S.N. (2022). Study of baffles arrangement influence on the natural convection into a heated square channel. Mathematical Modelling of Engineering Problems, 9(4): 1025-1030. https://doi.org/10.18280/mmep.090420
[17] Rebhi, R., Ahmad, H., Zhao, Y.H., Menni, Y., Lorenzini, G. (2023). Numerical assessment of an air-heat exchanger channel with staggered attached rectangular baffles and in-line detached square fins. Thermal Science, 27(1): 343-351. https://doi.org/10.2298/TSCI23S1343R
[18] Fadhala, K., Fayyadh, E., Mohammed, A. (2023) Experimental investigation on the thermal-hydraulic performance of channel with gradient metal foam baffles. FME Transactions, 51(1): 14-22. https://doi.org/10.5937/fme2301014F
[19] Alwatban, A., Othman, H. (2023). Numerical analysis of turbulent air flow dynamics in a rectangular channel with perforated nozzle-shaped vertical baffles. International Journal of Heat & Technology, 41(6): 1407-1416. https://doi.org/10.18280/ijht.410602
[20] Demartini, L.C., Vielmo, H.A., Möller, S.V. (2004). Numeric and experimental analysis of the turbulent flow through a channel with baffle plates. Journal of the Brazilian Society of Mechanical Sciences and Engineering, 26: 153-159. https://doi.org/10.1590/S1678-58782004000200006
[21] Alqahtani, S., Kaid, N., Haque, M.S., Menni, Y. (2024). Finite element method-based investigation of heat exchanger hydrodynamics: Effects of triangular vortex generator shape and size on flow characteristics. AIP Advances, 14(8): 085124. https://doi.org/10.1063/5.0222106

NOMENCLATURE

u	fluid velocity in x-direction $[m/s]$
v	fluid velocity in x-direction $[m/s]$
h_d	channel hydraulic diameter $[m]$
L	channel height $[m]$
W	channel width $[m]$
H	channel height $[m]$
s	baffle porosity $[m]$
P	pressure $[Pa]$
T	temperature $[K]$
Re	Reynolds number [-]
T	temperature $[K]$
U	fluid velocity $[m/s]$
k_f	thermal conductivity $[W/mK]$
h_x	convection heat transfer coefficient $[W/m^2K]$
Pr	Parndlt number
Nu_x	local Nusselt number of baffle's channel
Nu_0	Nusselt number of empty channel
f_0	friction coefficient of empty channel
f	friction coefficient of baffle's channel
TEF	Thermal Enhancement Factor

Greek letters

ρ	density [kg/m^3]
μ_l	molecular viscosity
τ_w	shear stress at the wall $[N/m^2]$
μ_l	molecular viscosity $[Pa.s]$
μ_t	turbulent viscosity$[Pa.s]$
c_μ	turbulent constant
σ_k	turbulent constant
ε_k	turbulent constant
$G_{1\varepsilon}$	turbulent constant
$G_{2\varepsilon}$	turbulent constant